Electronic Supplementary Material (ESI) for Physical Chemistry Chemical Physics.

Supplementary Information

Gas-phase vs Material-kinetic Limits on the Redox Response of Nonstoichiometric Oxides

Ho-Il Ji [ac], Timothy C. Davenport [a], Michael J. Ignatowich [ad], and Sossina M. Haile [*abcd]

[a] Materials Science and Engineering, Northwestern University, Evanston, IL 60208, USA

[b] Applied Physics, Northwestern University, Evanston, IL 60208, USA

[c] Materials Science, California Institute of Technology, Pasadena, CA 91125, USA

[d] Chemical Engineering, California Institute of Technology, Pasadena, CA 91125, USA

Relaxation Behavior of Porous Materials in the Surface Reaction Limit

Rapid bulk diffusion implies the absence of a concentration gradient within the solid phase, expressed as:

$$c_{\mathrm{O}}(\vec{r},t) = c_{\mathrm{O}}(t) \qquad \left(\vec{r} \in R\right) \tag{S1}$$

where $\vec{r}$ is the position variable and R is the region inside the oxide. In addition, at high flow conditions, the final $p\mathrm{O}_2$ surrounding the oxide, which drives the oxygen concentration to the new equilibrium state is fixed throughout the relaxation process. If, moreover, the surface reaction is first order in oxygen concentration, the oxygen flux (J) at the surface of and inside the oxide is

$$J(\vec{r},t) = \begin{cases} k_{\mathrm{Chem}}(t)\left[c_{\mathrm{O,f}} - c_{\mathrm{O}}(t)\right] & \left(\vec{r} \in S\right) \\ J(t) \approx 0 \qquad \left(\vec{r} \in R \text{ and } \vec{r} \notin S\right) \end{cases} \tag{S2}$$

where k_{Chem} is the surface reaction rate constant, $c_{\mathrm{O,f}} = c_{\mathrm{O}}(t = \infty)$, and S is the surface domain of the oxide.

In the absence of sources or sinks of oxygen, the rate of change in concentration in the volume element is determined by the flux of oxygen entering it (the continuity relation):

$$\frac{\partial c_{\mathrm{O}}(t)}{\partial t} = \frac{\partial J(\vec{r},t)}{\partial \vec{r}} \tag{S3}$$

The rate of change in concentration over the total volume of the oxide can be obtained by inserting Equation (S2) for the flux into Equation (S3) and then integrating, giving:

$$\int_R \frac{\partial c_{\mathrm{O}}(t)}{\partial t} dV = \int_S k_{\mathrm{Chem}}(t)\left[c_{\mathrm{O,f}} - c_{\mathrm{O}}(t)\right] dA \tag{S4}$$

$$\frac{\partial c_{\mathrm{O}}(t)}{\partial t} = \frac{k_{\mathrm{Chem}}(t)A}{V} \times \left[c_{\mathrm{O,f}} - c_{\mathrm{O}}\left(t\right)\right] \tag{S5}$$

where V and A are, respectively, the volume and surface area of the oxide. The solution to Equation (S5) has a simple exponential form. If the total conductance again changes linearly with oxygen concentration, the normalized conductance is then:

$$\frac{G(t) - G_{\mathrm{i}}}{G_{\mathrm{f}} - G_{\mathrm{i}}} = \frac{c_{\mathrm{O}}(t) - c_{\mathrm{O,i}}}{c_{\mathrm{O,f}} - c_{\mathrm{O,i}}} = 1 - \exp\left(-\frac{k_{\mathrm{Chem}}A}{V}t\right) = 1 - \exp\left(-\frac{t}{\tau}\right) \tag{S6}$$

where the time constant is now defined by

$$\frac{1}{\tau} = \left(\frac{k_{Chem}A}{V}\right) \tag{S7}$$

This result has been presented without derivation by Kim et al.[1]

log (1/τ) vs. 1/T behavior for ceria under gas-phase limitation

The reduction enthalpy and entropy of ceria were used to complete the correlation in all range of temperature and pO_2 vs. δ. The detail is explained in the previous study.[2] From the data set of $\delta(pO_2, T)$,[3] the value of $\log\left(-\frac{\partial pO_2(\delta,T)}{\partial\delta}\Big|_{\delta=\delta_f}\right)$ in Equation (2) is calculated at the fixed pO_2 of 8.2×10^{-4} atm. The result is depicted in Figure S1.

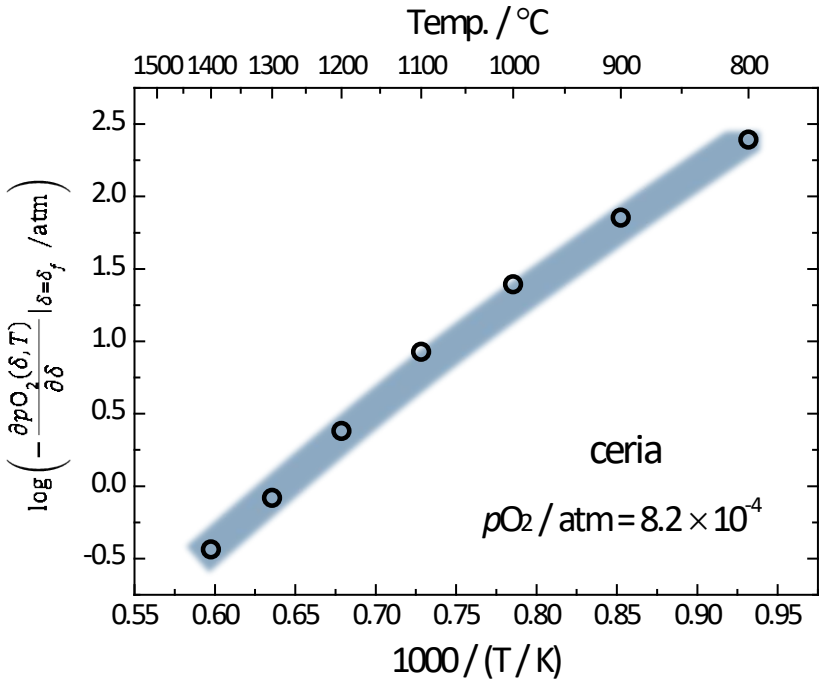

Figure S1. $\log\left(-\frac{\partial pO_2(\delta,T)}{\partial\delta}\Big|_{\delta=\delta_f}\right)$ **at a pO_2 of 8.2×10^{-4} atm as a function of temperature.**

Thermogravimetric analysis of ceria-based slurries

Thermogravimetry (TG) measurements were performed on polyurethane sponge (Foam-Partner, Fritz Nauer AG) and carbon powder (STREM chemicals, 93-0601, 325 mesh) with a mass of 110 and 41 mg, respectively, in a thermal analyzer (Netzsch STA 449 F5) using an alumina crucible. The sample heated up to 1000 °C at a ramp rate of 10 °C/min with flowing Ar (100 sccm) + air (30 sccm).

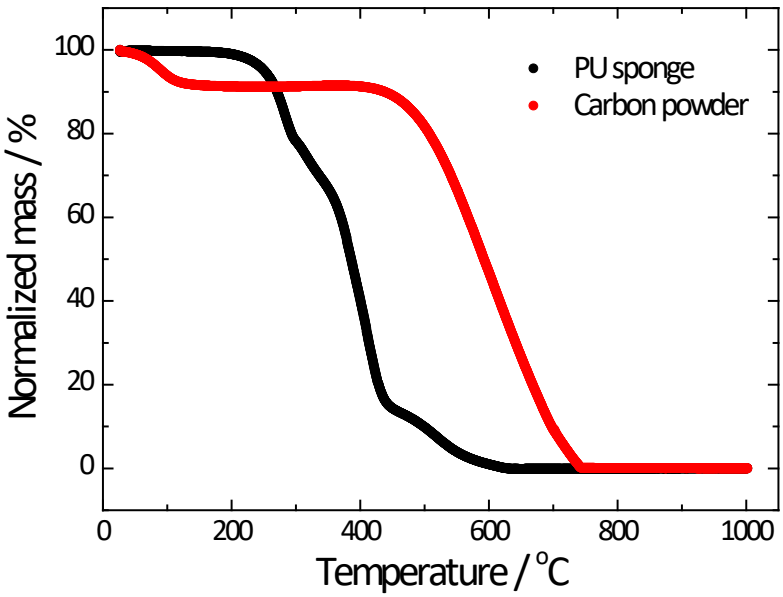

Figure S2. TGA profiles of polyurethane sponge and carbon powder.

Volume specific surface area measurements

Mercury Intrusion Porosimetry: RPC-00 and RPC-50 samples with a mass of 0.3316g and 0.4028g, respectively, were characterized by mercury intrusion porosimeter (Micromeritics Autopore V, USA). The specific surface area values were taken from the cumulative pore area.

X-ray Tomography: RPC-00 and RPC-50 samples were scanned at 2-BM beamline of Advanced Photon Source at Argonne National Laboratory. X-ray beam was filtered with 15-mm Si and 20-mm glass blocks. A sample was rotated in 0 - 180 degree angle range and x-ray projection images were taken at discrete angle position with 0.12 degree/step. The x-ray microscope is composed of a 20um thick LuAG:Ce scintillator, a 10x long working distance microscope lens (Mitutoyo Corp.), and a pco.edge camera. Tomographic slice images were reconstructed with Tomopy[4], and Avizo® was used for tomographic structure visualization and calculation of area-volume ratio.

Table S1. Volume specific surface area by Mercury porosity and X-ray tomography measurements

Sample	Mercury intrusion porosimetry (mm^{-1})	X-ray tomography (mm^{-1})
RPC-00	80	25
RPC-50	800	370

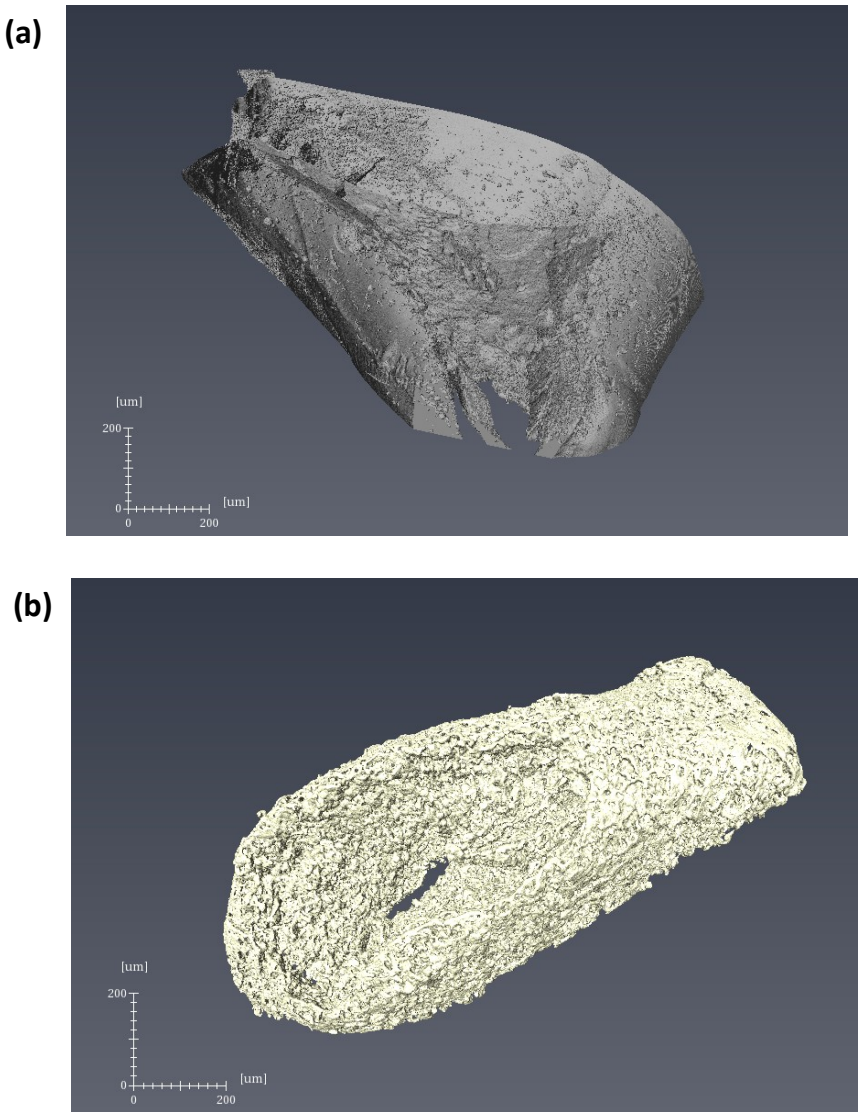

Figure S3. Reconstructed 3D images of preliminary X-ray tomography analysis for (a) RPC-00 and (b) RPC-50.

Experimental configuration for ECR measurements

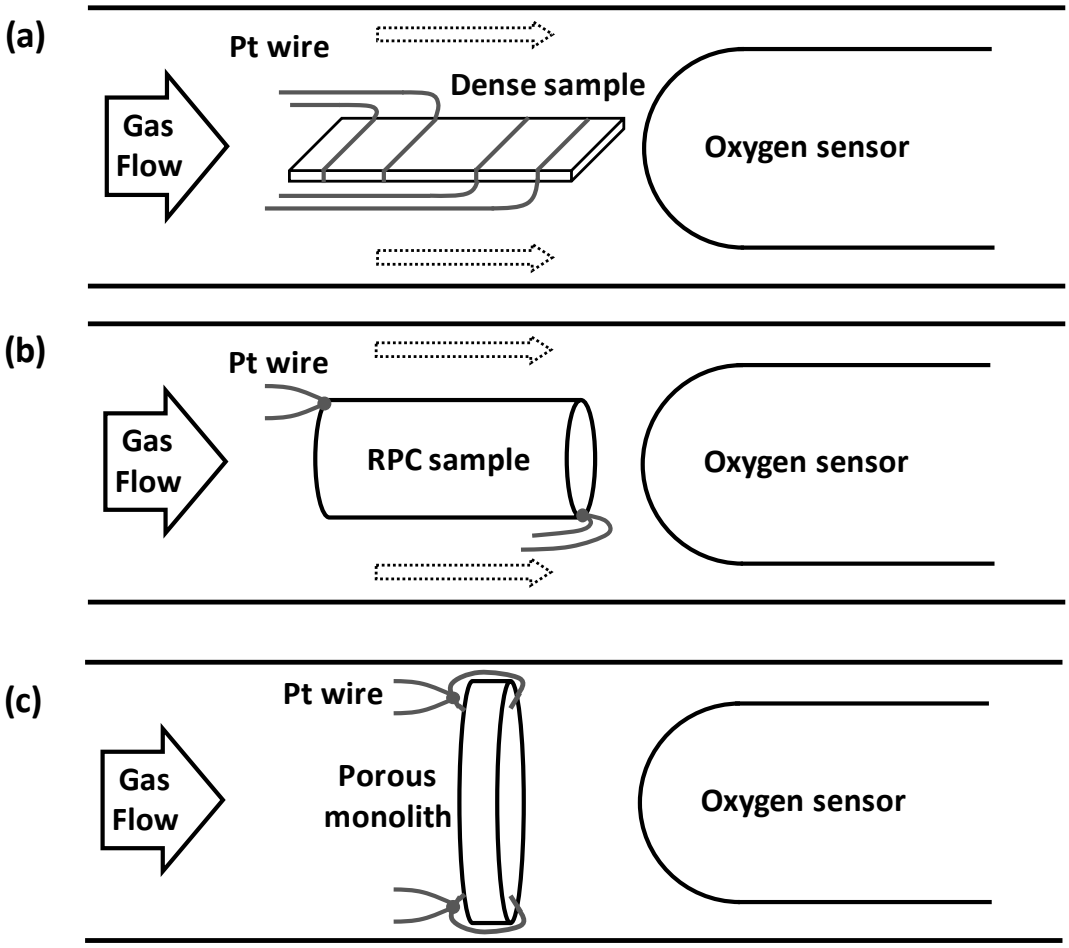

Figure S4. Schematics of electrical conductance relaxation test system: (a) dense polycrystalline bulk, (b) RPCs, and (c) porous monolith samples.

Relaxation profiles and surface reaction constant of dense ceria

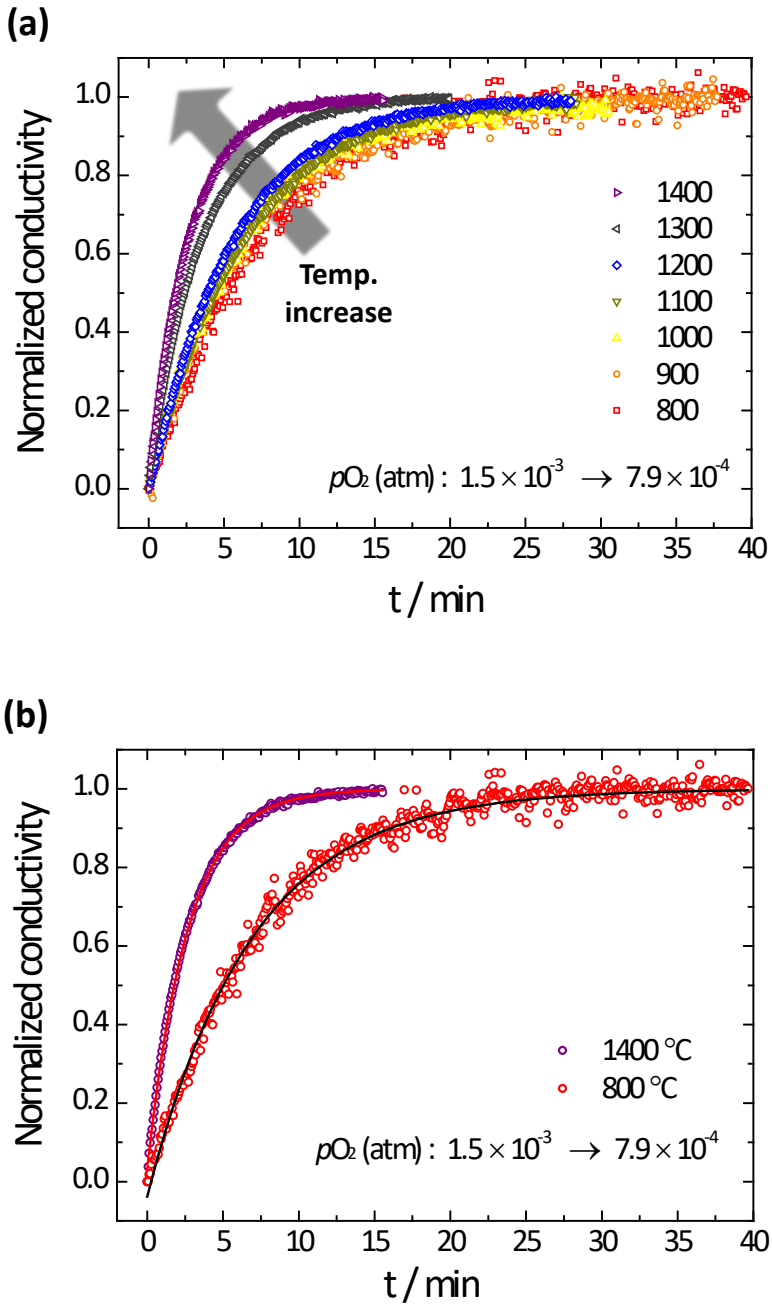

Figure S5. Conductivity relaxation profiles for bulk ceria under the small step change in pO_2 ($1.5 \times 10^{-3} \rightarrow 7.9 \times 10^{-4}$ atm) from (a) 800 to 1400 °C. (b) The profiles at 800 and 1400 °C are shown with the best fit result (solid lines).

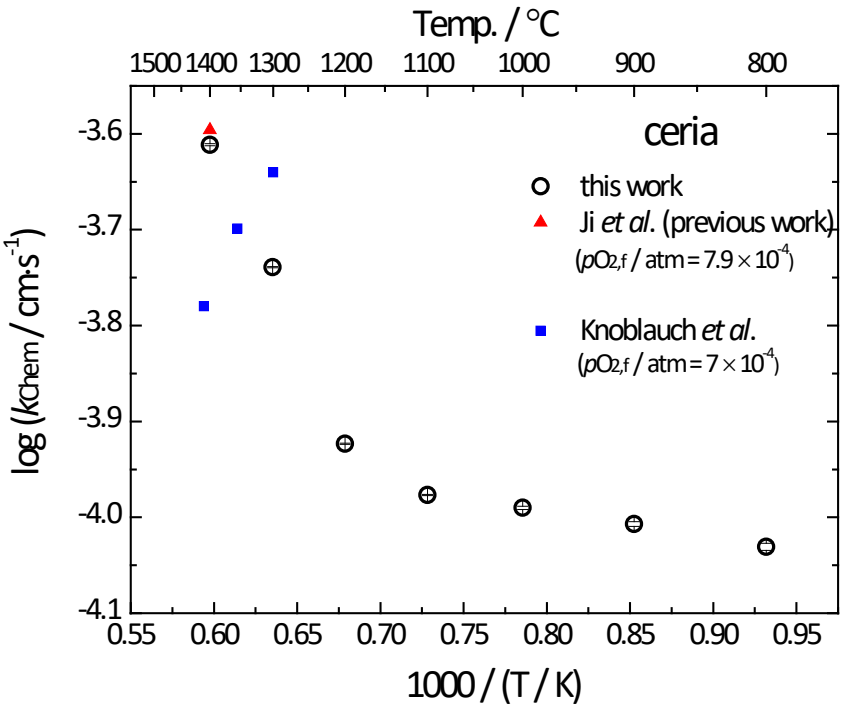

Figure S6. The surface reaction rate constant, k_{Chem}, for ceria as a function of temperature at sufficiently high flow rates (763 sccm/g). Shown for comparison is the result reported by Knoblauch *et al.*[5] and Ji *et al.*[6]

The surface reaction constant of ceria as measured here is shown in Arrhenius format in Figure S6, along with two other results reported in the literature. The single datapoint from Ji *et al.* (our earlier work)[6] derives from an ECR measurement at 1400 °C over a range of pO_2 values. The agreement with the present data is good, significant because the measurement is made using a different sample.

In addition to these k_{Chem} measurements, Kamiya *et al.* reported the value of k^*, obtained from isotope exchange methods, for temperatures from 800 to 1300 °C.[7] As discussed at some length in the literature, k_{Chem} and k^* measure different characteristics of a material, and computing one from the other requires knowledge of the thermodynamic factor ($d \ln a_O / d \ln c_O$, where a_O is oxygen activity and c_O is oxygen concentration) and

electronic transference number.[8] Nevertheless, it is noteworthy that Kamiya *et al*. observed a k^* that monotonically increased with temperature, showing a single slope in the Arrhenius representation [described according to k^* (m/s) = 1.93 × 10^{-3} exp[-136 (kJ·mol^{-1})/RT]. Somewhat surprisingly, those authors reported that their high purity undoped ceria exhibited extrinsic behavior below about 1000 °C, as manifest in a change in slope in the dependence of log (D_{Chem}) vs. 1/T, but with no comparable change in slope in the analogous plot for k_{Chem}. It would be reasonable to attribute the change in slope evident in Figure 5 of the present work in to a transition between intrinsic and extrinsic behavior given the comparable levels of impurities in the Kamiya and present samples. However, no attempt has been made here to prove or disprove such a hypothesis. Another possible explanation for the change in slope is impurity segregation to the surface-exposed grain boundaries layer[9-11]. It has been reported that such segregation can affect gas-solid reactions[12-14] and may be expected to play a role here as the present conductivity relaxation was performed using polycrystalline ceria with grain size of ~ 10 μm.

Also shown in Figure S6 are a set of three data points from Knoblauch *et al*. These authors measured the surface reaction constant by mass relaxation methods (in a conventional thermogravimetric analyzer) from 1300 to 1410 °C.[5] They reported that the surface reaction constant decreases with temperature, in sharp contrast to the present results. It is possible that this unusual observation is a result of performing measurements within the thermo-kinetic regime. The normalized gas flow-rate employed by those authors was 93 sccm/g at a pO_2 of 7 × 10^{-4} atm, and the quoted k_{Chem} at 1400 °C 1.69 × 10^{-4} cm/s. As implied by Equations (5)-(6) and discussed in detail in our earlier work[6], in order to ensure one is operating in the material-kinetic regime, the mass-normalized flow rate must obey

$$\frac{F}{m_{CeO_2}} > \frac{k_{Chem}}{a}\frac{P_{tot}}{2M_{CeO_2}}\left(-\left.\frac{\partial pO_2(\delta)}{\partial\delta}\right|_{\delta=\delta_f}\right)^{-1}$$

For the ~ 1 mm sample thickness and gas exchange occurring only from one side of the sample, the required flow rate is ~ 400 sccm/g, substantially greater than what the authors employed.

Behavior of time constant in a system maximizing the utilization of sweep gas

Support for the conclusion that insufficient interaction between the solid and gas phases results in a relaxation time in the thermo-kinetic regime that is larger than theoretically expected emerges upon examination of the correlation between the oxygen partial pressure detected at the downstream sensor, Figure S4, and the sample conductance. If the gas (upon entering the chamber) and the solid phases are entirely in equilibrium through the relaxation, and the step change in pO_2 is small enough that it induces a proportional change in conductance[15], then the oxygen partial pressure and conductance should depend on time in an identical manner. Thus, a plot of $G(t)$ vs. $pO_2(t)$ (a parametric function of time) should yield a straight line extending from the initial to the final values of the two quantities. The same is also true of a plot of the normalized logarithmic values, *i.e.*, $\frac{\log G(t) - \log G_\mathrm{i}}{\log G_\mathrm{f} - \log G_\mathrm{i}}$ vs. $\frac{\log pO_2(t) - \log pO_{2,\mathrm{i}}}{\log pO_{2,\mathrm{f}} - \log pO_{2,\mathrm{i}}}$, where the initial and final pairs of values are (0,0) and (1,1). This behavior is shown as the red line in Figure S8. If, however, the solid does not attain equilibrium with the gas as a consequence of slow surface reaction kinetics, and the gas flow is high enough that the gas composition is unaffected by adsorption or release of oxygen from the solid, then the oxygen partial pressure in the gas phase will immediately attain the final value (equal to the inlet value), whereas the conductance will require finite time to reach the final state. A plot of the normalized logarithmic values of conductance vs. oxygen partial pressure then follows the path (0,0) $\rightarrow$ (1,0) $\rightarrow$ (1,1), shown schematically in the dark blue lines of Figure S8. The intermediate case is that in which the gas-phase oxygen partial pressure is, at any given point in time, closer to its final value than the conductance is. This behavior is represented by the dotted curve in Figure S8. Such a response can be expected from a gas that does not fully

interact with the sample and, as a consequence, does not induce a change in conductance as quickly as the change in gas composition occurs.

Plots of normalized log conductance vs. normalized log pO_2 at 1400 °C are presented in Figure S9 for the three porous samples. At low gas flow-rates the porous monolith displays essentially ideal behavior for the gas-limited case, Figure S9(a). With an increase in gas flow rate, the behavior deviates slightly from the ideal case, Figure S9(b). The RPC-00 sample, Figure S9(c), which displays relaxation times furthest from the values implied from the thermodynamic properties of ceria, Figure 9, has a profile in the normalized log G vs. normalized log pO_2 plots which deviates most significantly from the idealized red line of . The RPC-50 sample, has intermediate behavior both in terms of the measured relaxation times, Figure 9, and the correlation between G and pO_2, Figure S8(d). Neither of the RPC samples displays the idealized profiles for the limit of material-kinetic controlled response, consistent with the fact that the relaxation has not yet reached the flow rate independent regime, Figure 7.

One can also consider the gas-solid interaction likelihood from the perspective of the gas diffusion dynamics. The gas-phase diffusion coefficient of O_2 at 1400 ^oC in the O_2-Ar mixture employed in this work is approximately 4.5 $cm^2 \cdot s^{-1}$.[16] To provide the gas from the periphery of the reactor sufficient time to traverse the ~ 2.4 mm annular gap, Figure S4(b) and come in contact with the ~ 10 mm long RPC samples, the gas velocity should be no greater than 9.1 $cm \cdot s^{-1}$ and hence the flow rate no greater than 76 sccm. The actual gas flow rates utilized in this study, up to 500 sccm, greatly exceeded this value. For measurement of the surface reaction constant, the need to limit the gas velocity to ensure sufficient time for gas-solid interaction conflicts with the requirement that the normalized gas flow rate exceed thermodynamic limit. As shown by the PM sample, these competing requirements can be addressed by creating structures that fill the cross-sectional area of gas flow. Overall, the

experimental observations are consistent with the interpretation that the relaxation times are prolonged in the RPC samples because of the poor interaction of the gas phase with the reactive solid, and underscore the importance of optimal design of gas flow patterns and porous material architecture for maximizing catalytic response.

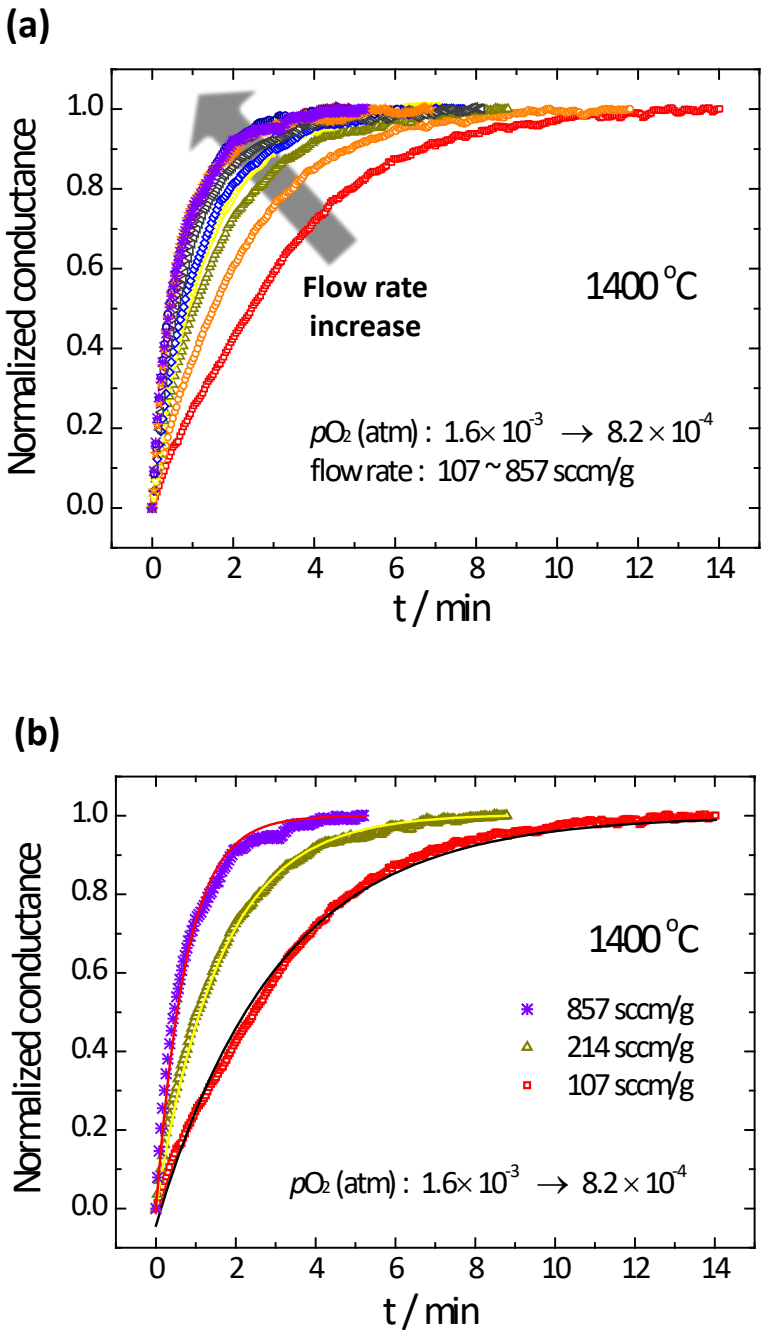

Figure S7. Conductance relaxation profiles for PM sample under a small step change in pO_2 ($1.6 \times 10^{-3} \rightarrow 8.2 \times 10^{-4}$ atm) at 1400 °C (a) in the range of the flow rate from 107 to 857 sccm/g. (b) The profiles at flow rates of 107, 214 and 857 sccm/g (50, 100, 400 sccm, respectively) are shown with the best fit result (solid lines).

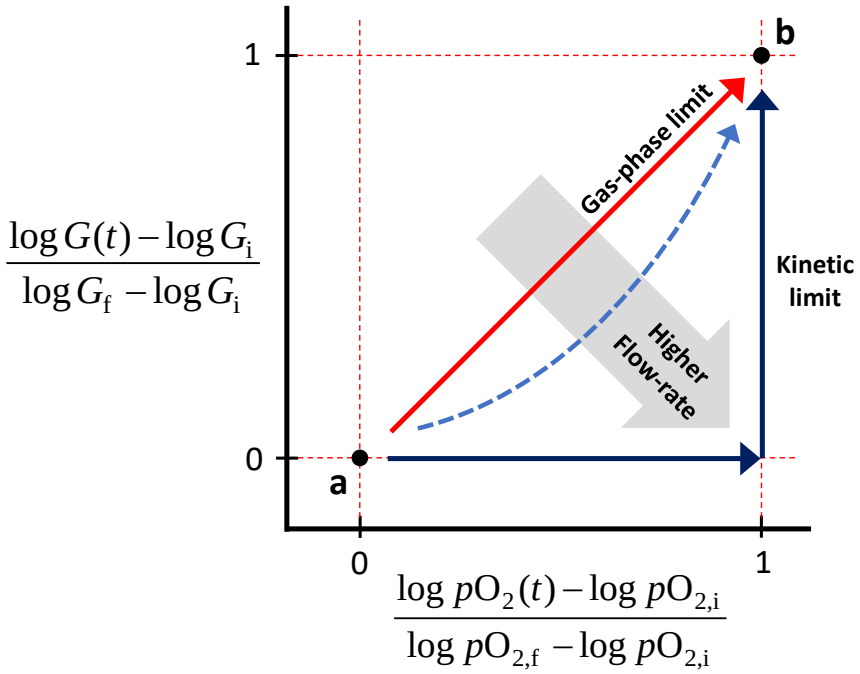

Figure S8. Changes of normalized log *G* vs. normalized log pO_2 with time at which the equilibrium state changes from "a" to "b".

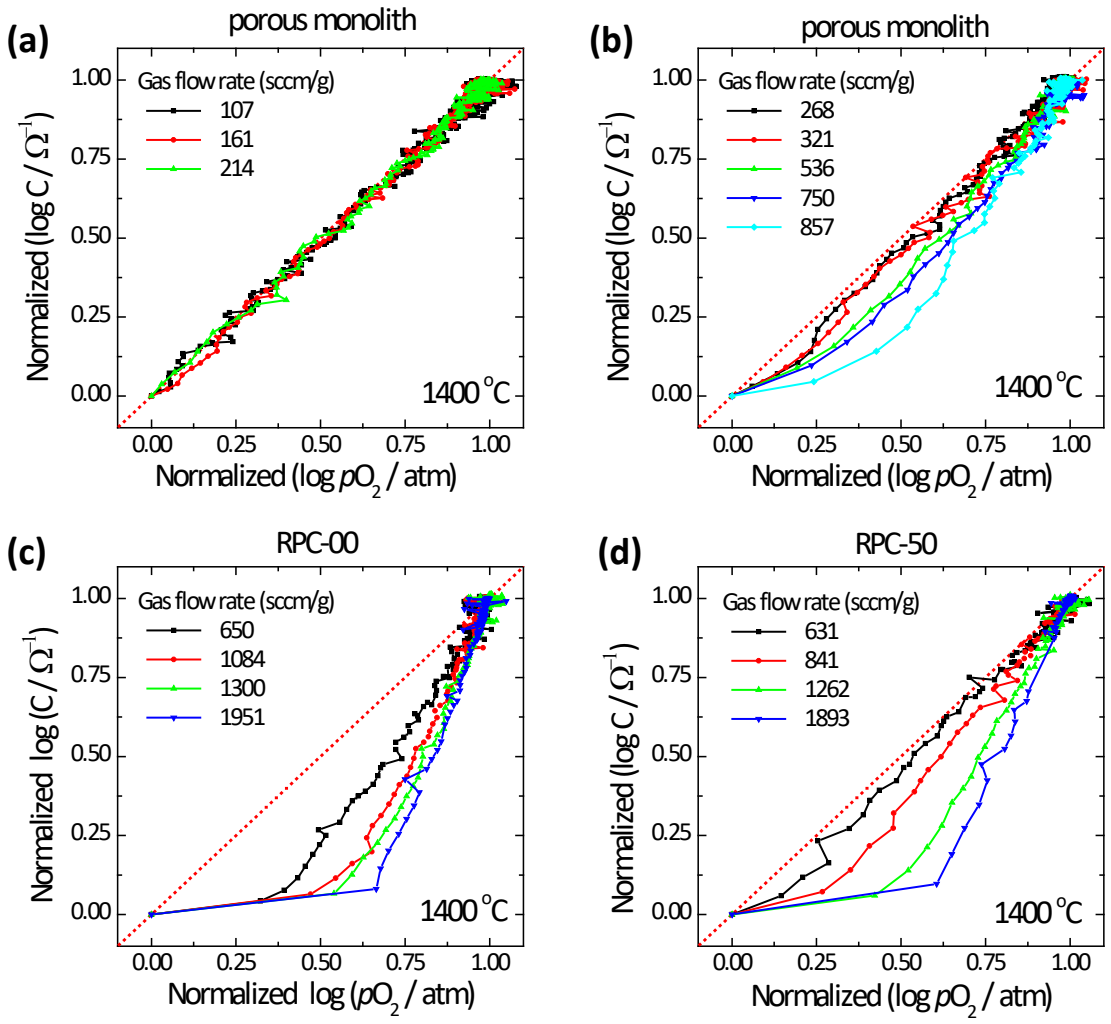

Figure S9. Normalized log *G* vs. normalized log pO_2 graphs at 1400 ºC for (a) porous monolith at low gas flow rates (107, 161, 214 sccm/g), (b) porous monolith at high gas flow rates (≥ 268 sccm/g), (c) RPC-00, and (d) RPC-50.

1. S. Kim, S. Wang, X. Chen, Y. Yang, N. Wu, A. Ignatiev, A. Jacobson and B. Abeles, *Journal of the Electrochemical Society*, 2000, **147**, 2398-2406.
2. T. C. Davenport, C. K. Yang, C. J. Kucharczyk, M. J. Ignatowich and S. M. Haile, *Energy Technology*, 2016, **4**, 764-770.
3. R. Panlener, R. Blumenthal and J. Garnier, *Journal of Physics and Chemistry of Solids*, 1975, **36**, 1213-1222.
4. D. Gürsoy, F. De Carlo, X. Xiao and C. Jacobsen, *Journal of synchrotron radiation*, 2014, **21**, 1188-1193.
5. N. Knoblauch, L. Dörrer, P. Fielitz, M. Schmücker and G. Borchardt, *Physical Chemistry Chemical Physics*, 2015, **17**, 5849-5860.
6. H.-I. Ji, T. C. Davenport, C. B. Gopal and S. M. Haile, *Physical Chemistry Chemical Physics*, 2016, **18**, 21554-21561.
7. M. Kamiya, E. Shimada, Y. Ikuma, M. Komatsu and H. Haneda, *Journal of the Electrochemical Society*, 2000, **147**, 1222-1227.
8. J. Maier, *Solid State Ionics*, 1998, **112**, 197-228.
9. R. Gerhardt and A. Nowick, *Journal of the American ceramic society*, 1986, **69**, 641-646.
10. R. Gerhardt, A. Nowick, M. Mochel and I. Dumler, *Journal of the American Ceramic Society*, 1986, **69**, 647-651.
11. J. Tanaka, J. F. BAUMARD and P. ABELARD, *Journal of the American Ceramic Society*, 1987, **70**, 637-643.
12. R. E. Usiskin, S. Maruyama, C. J. Kucharczyk, I. Takeuchi and S. M. Haile, *Journal of Materials Chemistry A*, 2015, **3**, 19330-19345.
13. W. Lee, H. J. Jung, M. H. Lee, Y. B. Kim, J. S. Park, R. Sinclair and F. B. Prinz, *Advanced Functional Materials*, 2012, **22**, 965-971.
14. E. Navickas, T. M. Huber, Y. Chen, W. Hetaba, G. Holzlechner, G. Rupp, M. Stöger-Pollach, G. Friedbacher, H. Hutter and B. Yildiz, *Physical Chemistry Chemical Physics*, 2015, **17**, 7659-7669.
15. H. Tuller and A. Nowick, *Journal of The Electrochemical Society*, 1979, **126**, 209-217.
16. J. R. Welty, C. E. Wicks, G. Rorrer and R. E. Wilson, *Fundamentals of momentum, heat, and mass transfer*, John Wiley & Sons, 2009.